

## Structural and Functional Evaluation of Glaucomatous Neurodegeneration from Eye to Visual Cortex using 1.5T MR Imaging: A Pilot Study

Kaya N Engin<sup>1\*</sup>, Bülent Yemişci<sup>2</sup>, Sibel Törezen Bayramoğlu<sup>3</sup>, Nurten Turan Güner<sup>3</sup>, Onur Özyurt<sup>4</sup>, Esin Karahan<sup>4</sup>, Cengizhan Öztürk<sup>4</sup> and Penbe Çağatay<sup>5</sup>

<sup>1</sup>Department of Ophthalmology, Ümraniye Education and Research Hospital, Istanbul, Turkey

<sup>2</sup>Department of Ophthalmology, Bağcılar Education and Research Hospital, Istanbul, Turkey

<sup>3</sup>Department of Radiology, Bakırköy Education and Research Hospital, Istanbul, Turkey

<sup>4</sup>Institute of Biomedical Engineering, Bogazici University, Istanbul, Turkey

<sup>5</sup>Department of Biostatistics and Medical Informatics, Istanbul Faculty of Medicine, Istanbul University, Istanbul, Turkey

\*Corresponding author: Kaya N. Engin MD, PhD, Department of Ophthalmology, Ümraniye Education and Research Hospital, Elmalıkent Mh. Ümraniye 34764, Istanbul, Turkey, Tel: ++90 216 6321818, ++90 506 7002599; Fax: ++90 216 632 71 24; E-mail: [kayanengin@hotmail.com](mailto:kayanengin@hotmail.com)

Received date: February 10, 2014, Accepted date: June 09, 2014, Published date: June 16, 2014

Copyright: © 2014 Engin KN, et al. This is an open-access article distributed under the terms of the Creative Commons Attribution License, which permits unrestricted use, distribution, and reproduction in any medium, provided the original author and source are credited.

### Abstract

**Aim:** Glaucoma is an optic neuropathy and glaucomatous damage proceeds from retinal ganglion cells to brain. A better understanding of retrobulbar damage will enable us to develop more efficient strategies and a more accurate understanding of glaucoma. We evaluated retrobulbar glaucomatous damage with favorable techniques for 1.5T MR imaging.

**Material and methods:** Five glaucoma cases and one healthy subject are included. Diffusion tensor MR imaging and functional MR images were taken with 1.5T MR. Correlation of optic nerve and corpus geniculatum laterale diffusion tensor MR parameters with eye findings were statistically evaluated.

**Results:** Optic nerve damage and cortical hypofunction were shown with diffusion tensor MR and functional MR imaging, respectively. Correlations of the apparent diffusion coefficient with mean deviation, pattern standard deviation, retinal nerve fiber layer thickness in distal optic nerve and fractional anisotropy with ganglion cell counting in proximal optic nerves and correlations of retinal nerve fiber layer thickness with axial diffusivities in both ipsilateral and contralateral corpus geniculatum laterales and with fractional anisotropy in ipsilateral corpus geniculatum laterale were statistically significant.

**Conclusion:** The eye-brain connection in glaucoma can be evaluated with routine clinical instruments. Our results also revealed the eye-to-visual-pathway integrity of glaucomatous neurodegeneration, which must be verified in larger series.

**Keywords:** Corpus geniculatum laterale; Diffusion tensor MR; fMRI; Glaucoma; Neurodegeneration; Optic nerve; Magnetic resonance imaging

### Introduction

Glaucoma represents a group of neurodegenerative diseases characterized by structural damage to the optic nerve and the slow, progressive death of retinal ganglion cells (RGCs). Although elevated intraocular pressure (IOP) is traditionally considered the most important risk factor for glaucoma, progressive visual field loss is still a prevalent symptom in cases with well controlled IOPs [1]. Today, areas beyond the retina and optic nerve are taken into consideration in glaucoma as well. If we briefly recall the anatomy, it is as follows: the retina, optic nerve, optic chiasm, optic tracts, corpus geniculatum laterale (CGL) including lateral geniculate nuclei (LGN), optic radiations and striate cortex. The lateral fibers originating from the temporal side of the globe directly pass the optic chiasm, while medial fibers originating from the nasal side cross over to the opposite hemisphere [2]. Gupta and Yücel have provided primary histopathological evidences –including degenerative and/or

neurochemical changes, which –are similar to those in neurodegenerative diseases, in the LGN [3] and changes in metabolic activity in both the LGN and visual cortex, in glaucoma patients [4]. Optic nerve and LGN shrinkage and cortical ribbon thickness reduction in the postmortem specimens of a glaucomatous patient have been reported by the same group [5].

In light of these findings, studies for *in vivo* demonstration of brain damage in patients with glaucoma accelerate. For this purpose, the most commonly used technology is magnetic resonance imaging (MRI). Functional MRI (fMRI) is the technique that led to the first key findings in the visual cortex have been obtained with it. Increase in neuronal activity is accompanied by changes in blood oxygenation that give rise to changes in the MR signal. The net reduction of deoxyhemoglobin during brain activity manifests in an increase in the MR signals known as blood oxygenation level dependent (BOLD) signals. Duncan et al. managed to demonstrate the reflection of a visual field (VF) defect in the cerebral cortex with this technique [6]. Another important technique for imaging visual pathways is Diffusion-Tensor MRI (DTI). It is based on the movement principle of fluids in the nerve. Such movement is known as anisotropic diffusion which depends on the structural environment of white matter.  $\lambda_1$  and

radial diffusivities [ $\lambda^{\perp}$ ] form anisotropy and it is estimated as the fractional anisotropy (FA) and apparent diffusion coefficient (ADC). Radial diffusivities can be expressed as a single value,  $\lambda^{\perp}$ . A nerve can be traced with anisotropy maps, a process referred to as “Tractography” [7]. The optical tract in humans can be imaged from CGL to the calcarine sulcus with this method [8]. It was shown for the first time that *in vivo* 6T-DTI can be successfully applied to detect axonal density changes occurring in a rat model of glaucoma [9]. Optic radiations and optic nerves of patients with glaucoma were also evaluated with 3T MRI [10,11].

Above, we mentioned the possibilities provided by recent medicine to assess retrobulbar glaucomatous damage. In current practice, however, we most frequently use optical coherences tomography [OCT] and VF, to structurally and functionally examine glaucomatous damage in the eye [12].

In our study, we aimed to develop methods convenient for 1.5 T MRI device, in order to use both in the diagnosis and follow-up of glaucoma and in studies with large case series, and finally to establish a reference for studies on the pathogenesis, follow-up, and treatment of glaucoma. Moreover, we examined those techniques with OCT and VF, in order to demonstrate the eye-brain connection in patients with glaucoma –in a small case series.

## Methods

Five patients with asymmetrical primary open angle glaucoma and one healthy subject are included in this study. Baseline demographic and ophthalmic information of the study participants were recorded

(Table 1). All the subjects were over 45 years of age and without any known additional ocular, neurological or systemic diseases. A complete ophthalmological examination was performed. IOPs and OCT data were taken with the Pascal Dynamic Contour tonometry (Nidek Inc.) and RTVue-100 fourier domain OCT (Optovue Inc.), respectively. Central 30-2 threshold SITA-Standard visual fields were taken with the Humphrey Field Analyzer Model 740i (Zeiss Inc.). Glaucomatous asymmetries are defined according to the VF Mean Deviation (MD), Pattern Standard Deviation (PSD) and OCT RNFL, GCC values; along with other clinical findings including best corrected visual acuities, IOPs, optic nerve head cupping ratios (c/d). The research adhered to the tenets of the Declaration of Helsinki. Approval from Bakırköy Education and Research Hospital, Ethics Committee, and informed consent from the subjects were obtained. Color Doppler ultrasonography was performed in the carotid, ophthalmic, posterior ciliary and central retinal arteries in order to eliminate ischemic pathology. While the VF, MD and PSD values of the patient were recorded for functional analysis, thereby hemodynamic activity assessment in the primary visual cortex was performed with fMRI. Structural analyses were completed by comparing, c/d, RNFL and GCC values with DTI findings. All the measurements are completed on the same week for each subject. Only average RNFL and GCC parameters were used. While the bilateral eyes of the patients were compared with each other and with the control, compatibility between structural and functional analyses of global and optic pathways was also evaluated. Correlations of clinical findings of each eye were analyzed not only with ipsilateral optic nerve and fMRI findings, but CGLs on both sides as well. DTI and fMRI procedures were performed with a 1.5T (Avanto Siemens Erlangen, Germany) MRI device.

	Age	Eye	c/d	RNFL (µm)	GCC (µm)	PSD (dB)	MD (dB)
Control (Male)	47	Right	0.02	102.90	94.30	1.33	1,12
		Left	0	102.94	97.09	1.56	0.04
Patient 1 (Male)	64	Right	0.18	102.80	109.25	2.18	-2.75
		Left	0.45	71.04	82.16	11.13	-22.15
Patient 2 (Male)	76	Right	0.89	71.57	76.63	7.14	-12.97
		Left	0.54	80.09	79.70	9.52	-13.5
Patient 3 (Male)	39	Right	0.98	64.52	81.15	14.23	-10.90
		Left	0.93	69.81	78.5	7.10	-19.55
Patient 4 (Male)	56	Right	0.71	111.26	101.88	6.75	-6.23
		Left	0.63	108.77	104.07	4.94	-5.57
Patient 5 (Female)	15	Right	0.18	110.36	105.14	1.73	-1.52
		Left	0.22	114.86	107.68	6.81	-3.90

c/d: Optic nerve head cupping ratios; RNFL: Retinal Nerve Fiber Layer Analysis; GCC: Ganglion Cell Counting; PSD: Pattern Standard Deviation; MD: Mean Deviation

**Table 1:** Baseline demographic and ophthalmic information of the study participants.

## DTI imaging

Imaging protocol consisted of obtaining a high resolution T1 weighed (1×1×1 mm) MPRAGE sequence, as well as fMRI time series images and diffusion weighed images. Diffusion weighed images in 30 different directions and with two different b values (b=0.1000) were

obtained. Imaging parameters were determined as TR=8200 ms, TE=90 ms, 2 mean, 3×3×3 isotropic voxel dimensions, a total of 60 slices, and an imaging duration of approximately eight minutes. Diffusion weighed images were first separated from non-brain sections using FSL software. Using MedINRIA software on those images,

diffusion tensor maps and fiber tractographs were created. Moreover, magnification was applied on b0 coronal plane images obtained from the same region and optic nerve morphologies were also evaluated on this plane.

### DTI data analysis

In three planes, proximal and distal regions of interest (ROI)s were selected on the optic nerve at about 3 mm and 8 mm distances from the globe, respectively (Figure 1A). DTI parametric values FA, ADC,  $\lambda_1$ ,  $\lambda_2$ ,  $\lambda_3$  of the optic nerves were calculated. Parameters were also calculated in CGL areas with a semiautomatic marking technique. DTI maps obtained from the control and the patients were overlapped with a standard DTI image described in MNI152 space by order of in linear (FLIRT) and nonlinear (FNIRT) fashions [13,14]. Each CGL was marked with the help of Jülich Histological atlas [15] in the same standard space [16]. Those regions were selected -and retouched when necessary, by experienced radiologists (Figure 1B).

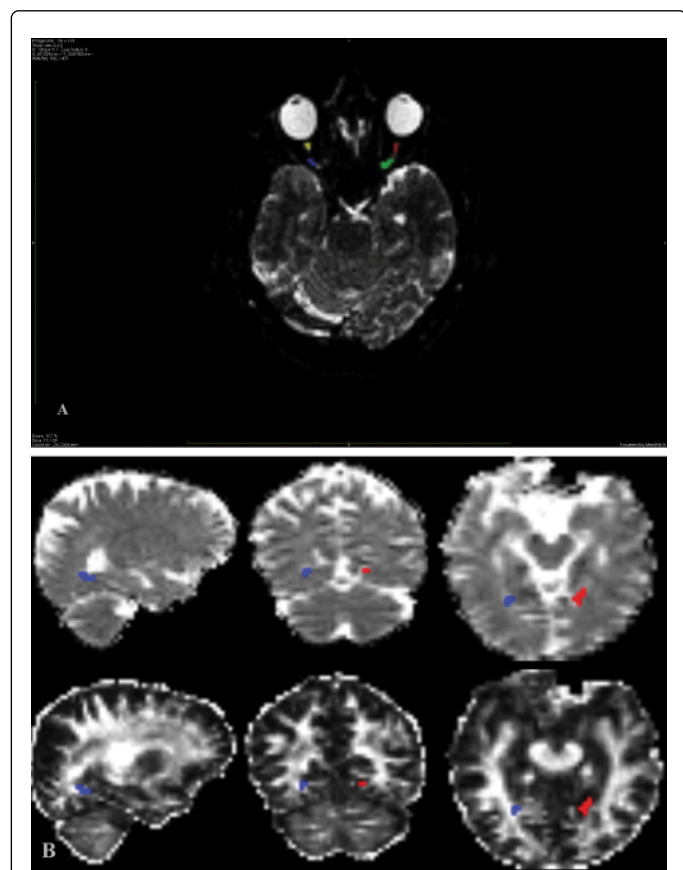


**Figure 1:** ROI determination from proximal and distal optic nerves (in four colors) (A), ipsilateral and contralateral corpus geniculatum laterales (in blue) (B) for diffusion analysis with DTI.

### fMRI imaging

An anatomic image was obtained in 128 slices in 1×1×1 mm resolution with a high resolution T<sub>1</sub> weighed 3D GRE sequence. Functional MRI images were obtained with a T<sub>2</sub> weighted GE-EPI sequence. In a 64×64 data collection matrix, 29 axial slices covering the visual cortex were obtained at resolution of 3×3×3 mm voxel

dimensions. TR was 2800 ms, TE was 30 ms and the flip angle was 90 degrees. Two consecutive recording sessions were performed for the left and right eyes of the patients with glaucoma. Thus, 544 volumes, including 272 volumes for each eye, were obtained from each individual.

### Stimulation

The left and right eyes were stimulated separately in each session. Visual stimuli -from the programmed- OpenGL library were displayed by reflecting images onto a mirror inside the MRI machine via an LCD projector and transparent curtain during the experiment. The visual field angle was measured as 40° on a horizontal plane and 25° on a vertical plane. The visual field was divided into five rings, each consisting of 12 sectors, and small spaces were left in order to differentiate each sector from the other. During the experiment, subjects were asked to focus on the center point of the stimulation. Half of the selected 60 regions in the visual field along 67 blocks were flashed at a frequency of 8 Hz in the form of 4×4 chess boards (Figure 2) [17].

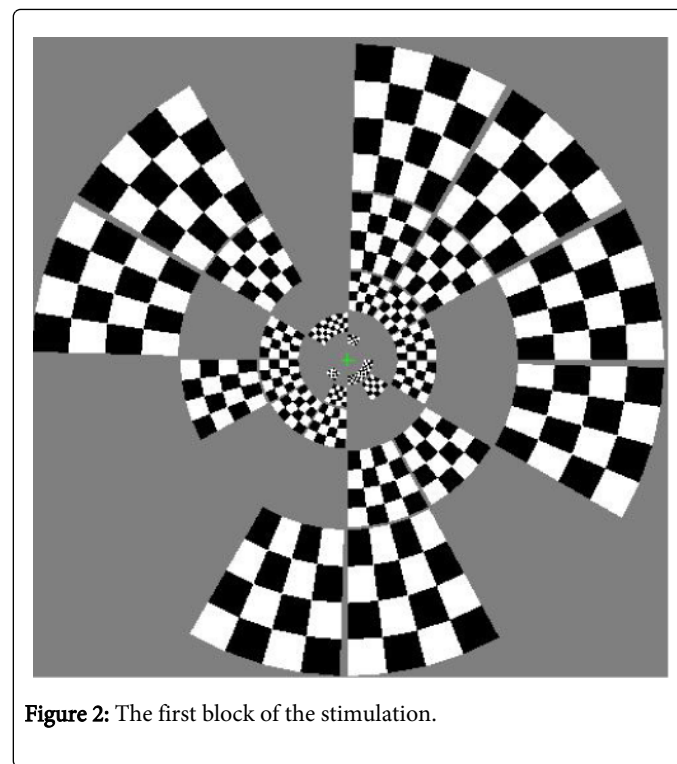


**Figure 2:** The first block of the stimulation.

### fMRI data analyses

Functional analyses were performed with SPM5 (Wellcome Department of Imaging Neuroscience, London, England). Following standard movement correction and slice time correction procedures, all functional images were blurred using a Gaussian spatial filter with FWHM of 5 mm. To model the fMRI signal, we used a regressor for each of 60 regions and after convolving with hemodynamic response function these regressors were used in general linear model.

For each of the 60 regions divided on the visual field, SPM(t) maps were created that provided information on the activation in relevant regions. Those maps were masked in the form of ( $t > 3.12$ ,  $p < 0.001$ ). In order to compare activations occurring in the visual cortex, the visual

field regions most heavily influenced by glaucoma were determined in each patient, and activations occurring in the stimulation of those regions were calculated. For this purpose, voxel clusters exceeding the cut-off value in SPM(t) maps of each region were found, and the percent change in BOLD was measured corresponding to those clusters.

### Statistical analysis

Statistical analyses were conducted using SPSS 17.0 software. Normality of data was evaluated by the Shapiro-Wilk test. Spearman's correlation coefficient ( $r_s$ ) was determined where appropriate. p values

less than 0.05 were considered significant. For the interpretation of correlation coefficients, values between 0.0-0.24, 0.25–0.50, 0.51–0.75 and 0.76–0.95 were considered as no correlation, weak, moderate and strong correlations, respectively.

### Results

In examinations performed with a Color Doppler ultrasonography, no vascular anomaly was observed. No additional ophthalmic pathology was detected with ophthalmic examination, and IOPs of all subjects were below 20 mmHg.

		FA	ADC (mm <sup>2</sup> /s)	$\lambda_1$ (mm <sup>2</sup> /s)	$\lambda_{\perp}$ (mm <sup>2</sup> /s)
Control	Right Ant	0.154404	9.1873	3.58415	2.80158
	Right Pst	0.208702	6.95286	2.84567	2.0536
	Left Ant	0.15729	9.1027	3.53808	2.78231
	Left Pst	0.237172	7.59813	3.17238	2.21287
Patient1	Right Ant	0.379233	4.00406	1.86058	0.52682
	Right Pst	0.616205	2.58347	1.55855	0.51201
	Left Ant	0.319462*	4.21222	1.89893	1.15665
	Left Pst	0.418491*	2.83058	1.36332*	0.73144
Patient 2	Right Ant	0.205464*	5.78025	2.3309*	1.65786
	Right Pst	0.22643*	5.55162	2.2359	1.72466
	Left Ant	0.257416	5.40597	2.28105	1.56246
	Left Pst	0.313278	4.67591	2.09265	1.29163
Patient 3	Right Ant	0.208077	6.41972	2.61022	1.90475
	Right Pst	0.201206	5.76068	2.29949	1.73060
	Left Ant	0.166546	6.49451	2.50869	1.99291
	Left Pst	0.303654	4.37636	1.90081	1.23778
Patient 4	Right Ant	0.175592	6.89216	2.70575	2.09320
	Right Pst	0.452029	3.57965	1.82854	1.02241
	Left Ant	0.238889	5.63989	2.36542	1.63724
	Left Pst	0.406642	3.96563	1.923	0.86901
Patient 5	Right Ant	0.244727	5.6688	2.40823	1.63029
	Right Pst	0.361881	4.58998	2.19107	1.19946
	Left Ant	0.156674	7.20704	2.76999	2.21853
	Left Pst	0.338958	5.83704	2.6748	1.55811

FA: Fractional Anisotropy;  $\lambda_1$ : Axial diffusivity;  $\lambda_{\perp}$ : Radial diffusivity

Grey areas and \* represent the eyes with severe glaucoma and reduction in the parameter, respectively

**Table 2:** Diffusion analysis findings of the control and the patient.

### Structural evaluation

**DTI imaging:** For the within subjects comparison, variable volume values were found. In comparison with each patient's fellow eye, a decrease in thickness and deterioration in the optic nerve diffusion of severely glaucomatous eyes of patients with asymmetrical involvement were observed in both b0 coronal plane images and optic nerve tractographies (Figure 3A and 3B). In DTI analysis, reduction in FA values in the eye with severe glaucoma relative to the fellow eye was observed in the patients with asymmetrical involvement (Table 2).

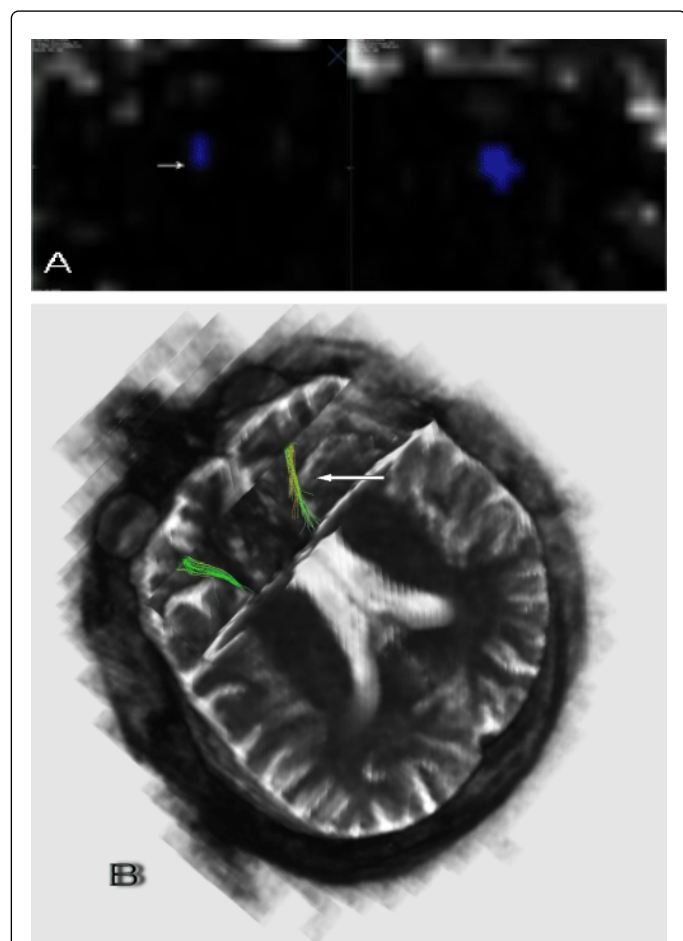


**Figure 3: Imaging of glaucomatous neurodegeneration in optic nerves.** (A) Temporal nerve fiber loss can be seen in the severely affected eye (arrows) in b0 coronal plane images of an asymmetrical patient (B) Isotropy and irregularity (arrows) in the optic nerve tractographies in the severely affected eye.

**DTI data analysis:** A decrease in MD was found to be correlated with optic nerve-1  $\lambda_1$ , ADC and optic nerve-2  $\lambda_1$  values. A PSD increase and a RNFL loss were also correlated with optic nerve-1 ADC values while a loss of GCC was correlated with optic nerve-2 FA values. Correlations of ADC with MD, PSD and RNFL in optic nerve-1 and FA with GCC in optic nerve-2 were statistically significant. In the DTI analysis CGLs, FA,  $\lambda_1$ ,  $\lambda_1^\perp$  values showed negative correlation with MD values on the same side and with RNFL values for both sides. Correlations of RNFL with  $\lambda_1$  on both sides and with FA in ipsilateral CGL were statistically significant (Table 3).

**Functional evaluation:** In fMRI analyses, data analyses were performed with reference to VF obtained in subjects. In the sensitive field analysis, success could not be gained since BOLD could not be obtained in all voxels and no significant correlation was observed with either OCT or VF findings (Table 3). In comparative analyses on quadrants with VF defects, in the patient with asymmetrical involvement, BOLD values were lower in the eyes with more defects than those of the other eyes (Figure 4).

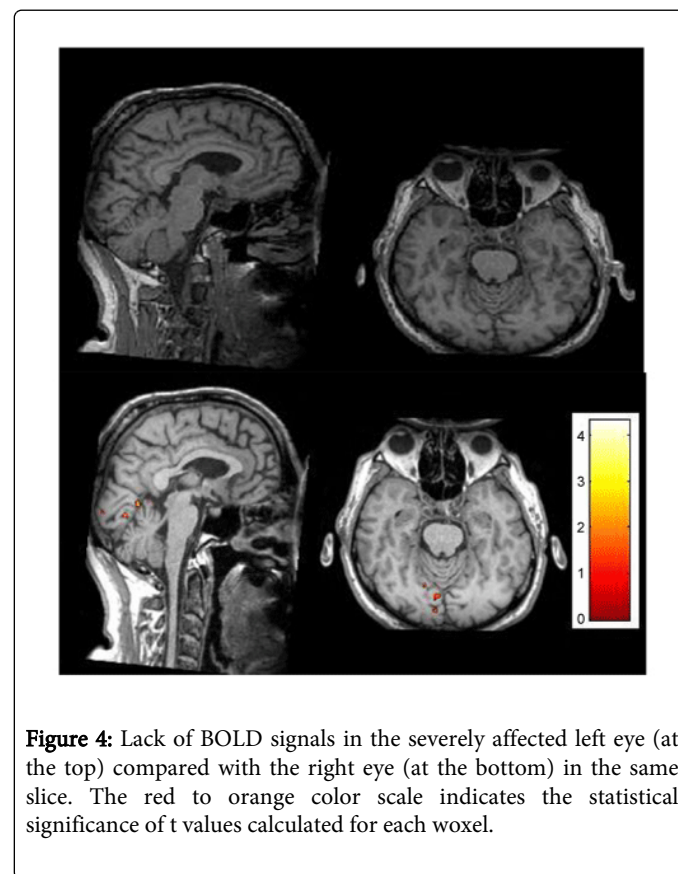


**Figure 4: Lack of BOLD signals in the severely affected left eye (at the top) compared with the right eye (at the bottom) in the same slice. The red to orange color scale indicates the statistical significance of t values calculated for each voxel.**

		MD-rs	p	PSD-rs	p	c/d-rs	p	RNFL-rs	P	GCC-rs	p
ON-1	FA	-.378	.226	.308	.331	.102	.753	-.287	.366	.105	.746
	ADC	.657	.020*	-.629	.028*	-.417	.178	.608	.036*	.238	.457
	$\lambda_1$	.538	.071	-.399	.199	-.214	.505	.378	.226	.070	.829
	$\lambda_1^\perp$	.434	.159	-.329	.297	-.130	.688	.301	.342	.070	.829

ON-2	FA	-.077	.812	-.140	.665	-.168	.601	.420	.175	.615	.033*
	ADC	.434	.159	-.168	.602	-.249	.436	.091	.779	-.210	.513
	$\lambda_1$	.573	.051	-.294	.354	-.312	.324	.196	.542	-.063	.846
	$\lambda^\perp$	.322	.308	-.070	.829	-.105	.745	-.084	.795	-.392	.208
CGL-I	FA	-.566	.055	.441	.152	.112	.729	-.580	.048*	-.350	.265
	ADC	.510	.090	-.420	.175	-.203	.527	.322	.308	.098	.762
	$\lambda_1$	-.573	.051	.483	.112	.133	.680	-.650	.022*	-.378	.226
	$\lambda^\perp$	-.636	.026*	.483	.112	.224	.484	-.538	.071	-.336	.286
CGL-C	FA	-.343	.276	-.315	.245	.260	.441	-.612	.060	-.315	.319
	ADC	.476	.118	.364	.319	-.191	.573	.200	.580	.119	.713
	$\lambda_1$	-.378	.226	.385	.217	.287	.392	-.673	.033*	-.364	.245
	$\lambda^\perp$	-.413	.183	.420	.175	.269	.424	-.588	.074	-.273	.391
BOLD	Max-min	.301	.342	-.343	.276	-.217	.498	.497	.101	.105	.746
	Max	.284	.372	-.333	.291	-.211	.511	.473	.121	.077	.812

Grey areas and \* represent statistically significant correlation and p values respectively. RNFL: Retinal Nerve Fiber Layer Analysis; GCC: Ganglion Cell Counting; MD: Mean Deviation; PSD: Pattern Standard Deviation; c/d: Optic nerve head cupping ratios; ON-1: Distal Optic Nerve; ON-2: Proximal Optic Nerve; CGL-I: Ipsilateral Corpus Geniculatum Laterale; CGL-C: Contralateral Corpus Geniculatum Laterale; FA: Fractional Anisotropy; ADC: Apperent Diffusion Coefficiency;  $\lambda_1$ : Axial Diffusivity;  $\lambda^\perp$ : Radial diffusivity; rs: Spearman's correlation coefficient

**Table 3:** Correlation of DTI and fMRI results with OCT and VF findings.

## Discussion

Studies focused on the glaucoma-brain connection have shown us that, diffusion of neurodegeneration in the brain should be taken into consideration in the diagnosis and follow-up of glaucoma [18]. The main aim of this study was to develop a method compatible with devices routinely used in clinics, because we believe that large case series can only be obtained with this approach. 1.5T MRI is routinely used in clinics by many disciplines.

The DTI examination, the structural examination arm of our study, was performed in two stages. In DTI diffusion analyses, no significant difference was obtained in the control relative to the patient values. That can be explained on the basis that the structure and diameter of the optic nerve may have significant (in the range of 4-9 mm) inter-individual variation [19]. On the other hand, the observed reduction in FA values in the optic nerve of the severely glaucomatous eye of patients with asymmetrical involvement compared with the less affected eye is compatible with the literature. In a DTI study with 7T MRI, experimental glaucoma was performed on seven rats, whereas the left eye served as the control. A decrease in FA values and an increase in  $\lambda_1$  values were observed in the glaucomatous eye's optic nerve and an increase in  $\lambda_1$  between Day 8 and Day 21 was found to be statistically significant [9]. In a study conducted on 16 patients with POAG, an increase in mean diffusivity values in addition to a decrease in FA values in both optic radiation s and optic nerves, were reported also parallel to our findings [10]. In a clinical study, a FA decrease along with an increase in  $\lambda$  values was reported in 30 patients [20].

In the second stage of DTI outcomes, morphological findings of -optic nerve deformation, which were visible in both OT and B<sub>0</sub> coronal plane images, are also compatible with the literature. The optic

nerve is of specific importance since it is among the structures most heavily influenced by glaucomatous neuro-degeneration and it provides information on the ipsilateral eye. In a study conducted with conventional MRI in patients with glaucoma, it was reported that the diameter of the optic nerve was significantly lower than that of the controls [21]. In the study of Hui et al., as much as a 10% decrease in axonal density of the glaucomatous optic nerve was detected in enlarged B<sub>0</sub> coronal plane images, which were also histopathologically confirmed [9]. Moreover, we imaged the temporal loss in severely affected optic nerves. Our findings were supported by two clinical studies as well. Lagreze et al. measured the diameter of retrobulbar optic nerves with an ultrafast high-resolution MRI at 3T. Included in the study were 38 glaucomatous, and nine healthy eyes [22]. Similar findings were obtained with 3T-DTI in 38 subjects [23].

Although, small sample size is a major limitation for our study, we obtained statistically significant data in the DTI analysis to evaluate the direct correlation between eye and central nerve system findings. MD and RNFL values were found to reflect the retrobulbar neurodegeneration more accurately than other parameters. Axon portion of RNFL thickness is proportional to local field sensitivity loss [24], and the recently recognized view is that, glaucomatous damage affects both structure and function in linear proportions [12,25]. A negative correlation between the mean FA for the optic nerves and glaucoma stage was reported [10]. According to two recent studies, -the optic nerve diameter was most closely related to the retinal nerve fiber layer thickness measured by an OCT [22,23]. In our study, optic nerve-1 diffusion parameters were found to be more closely correlated with OCT and VF findings. This is also consistent with the recent study of Bolacchi et al. in which, proximal optic nerve findings were

found to be more closely correlated with OCT data in early stage glaucoma [26].

A defect in the visual field may originate from pathology in any location ranging from the retina to the cortex [27]. It was reported that in normotensive glaucoma, a brain MRI revealed deeper depressions in the VF of a patient with ischemia [28]. In our study, we used fMRI to evaluate the visual cortex functionally, however, VF defects were found to be correlated with DTI findings. In the first study in the literature where a functional analysis with VF and MRI was conducted in glaucoma patients [6], the imaging of a defect of VF in the brain with 3T MRI using a long and complex stimulation was achieved. It is also possible to perform those precise analyses using our multifocal mapping method; however, 3T MRI was used in the original method [29]. In our study, since BOLD could not be obtained in all voxels in the sensitive area analysis with 1.5T MRI, a reliable data for correlation analyses could not be gained; however, an occipital cortex BOLD activity difference could be demonstrated in the highly asymmetrical patients. In the comparative analysis of quadrants with VF defects, it was found that BOLD values of the eye with serious defects were lower than those of the other eye.

Although CGL is one of the unique structures that histopathological studies have shown to be related to significant glaucomatous damage [5], there are few studies regarding either the clinical evaluation of glaucomatous CGL or the correlation of diffusion analyses with findings of eye. It is possible to obtain direct measures of functional cerebral blood flow changes with Arterial Spin Labeling fMRI [30]. Imaging of CGL structure with DTI, however, is debatable for it is not composed of intact white matter. CGL is a unique neural structure that is covered by the fibers of the optic tract, and serves as a processing station on the way from the retina to the occipital lobe of the cerebral cortex. It shows six cellular laminae, three of which are devoted to crossed fibers and the other three to uncrossed fibers [31]. CGL in humans was imaged using DTI, but no diffusion analysis has been performed [8]. Complex neural structures like basal ganglia and thalamus have also been imaged and water diffusivities of both white and gray matters have been successfully analyzed with DTI [32]. In another DTI study, lower FA of the left LGN have been reported in patients with migraines [33].

To our knowledge, two recent studies exist in the literature regarding glaucomatous CGL damage. In a preliminary study similar to ours, Zikou et al. combined voxel-based morphometry with DTI and revealed a significant reduction in the left visual cortex volume, the left lateral geniculate nucleus, and the intracranial part of the optic nerves and the chiasma [34]. Zhang et al. also reported a reduction in the left lateral geniculate nucleus volume, which was correlated with reduced RNFL thickness [20]. In this study, we did not include volume measures of any structure for we found it reliable to obtain DTI analysis from the safely selected ROIs. Interestingly, values we obtained from CGLs showed a negative significant correlation with MD values on the same side and with RNFL values of both sides. In complex neural structures, diffusion anisotropy is influenced by several factors including the degree of myelination, density, diameter distribution, diffusion balance between gray and white matter and orientational coherence of axons [33]. Although our findings have internal consistency, either verification in a larger series or illumination with further DTI studies is needed in order to draw conclusions.

Strategies independent from IOP, concerning the area beyond the optic nerve head, are needed in the evaluation and treatment of

glaucoma [1,34]. Currently, it is possible to image visual pathways from the optic nerve to the cerebral cortex both structurally and functionally. As our study showed, routine clinical instruments are also adequate for clinical trials to reveal the glaucoma-brain connection; however, more sophisticated techniques are being developed to illuminate that relation further. Our study also revealed a direct correlation between eye and central nerve system findings. Although these results imply the eye-to-visual-pathway integrity of glaucomatous neurodegeneration, that must be verified in larger series. Along with the limitation of the small sample size, the elevated number of correlation analyses highly inflated the Type I error (i.e., the probability of obtaining a statistically significant correlation coefficient by chance alone), thus affecting the results and conclusions of the study [35].

After many years of subsequent studies on glaucoma-brain connection, Gupta and Yucel conclude that glaucoma as a neurodegenerative disease is a valid working hypothesis to understand neural injury in the visual system, and this paradigm may stimulate the discovery of innovative IOP-independent strategies to help prevent loss of vision in glaucoma patients [3]. A more comprehensive understanding of retrobulbar glaucomatous damage will enable us to determine more efficient diagnosis, follow-up and treatment strategies and facilitate to answer important questions which remain unknown about this disease.

## Acknowledgement

Authors wish to thank Zafer Çukurova, MD and Cengizhan Öztürk MD, Prof for their enthusiastic contributions to this study.

## References

1. Weinreb RN (2007) Glaucoma neuroprotection: What is it? Why is it needed? *Can J Ophthalmol* 42: 396-398.
2. Sadun AA, Glaser JS, Bose S (2007) Anatomy of the visual sensory system. In: Tasman W, Jaeger EA (Eds), *Duane's Ophthalmology*. Lippincott Williams & Wilkins, Philadelphia.
3. Gupta N, Yücel YH (2007) Glaucoma as a neurodegenerative disease. *Curr Opin Ophthalmol* 18: 110-114.
4. Gupta N, Yücel YH (2003) Brain changes in glaucoma. *Eur J Ophthalmol* 13 Suppl 3: S32-35.
5. Gupta N, Ang LC, Noël de Tilly L, Bidaise L, Yücel YH (2006) Human glaucoma and neural degeneration in intracranial optic nerve, lateral geniculate nucleus, and visual cortex. *Br J Ophthalmol* 90: 674-678.
6. Duncan RO, Sample PA, Weinreb RN, Bowd C, Zangwill LM (2007) Retinotopic organization of primary visual cortex in glaucoma: Comparing fMRI measurements of cortical function with visual field loss. *Prog Retin Eye Res* 26: 38-56.
7. Nucifora PG, Verma R, Lee SK, Melhem ER (2007) Diffusion-tensor MR imaging and tractography: exploring brain microstructure and connectivity. *Radiology* 245: 367-384.
8. Sherbondy AJ, Dougherty RF, Napel S, Wandell BA (2008) Identifying the human optic radiation using diffusion imaging and fiber tractography. *J Vis* 8: 12.
9. Hui ES, Fu QL, So KF, Wu EX (2007) Diffusion tensor MR study of optic nerve degeneration in glaucoma. *Conf Proc IEEE Eng Med Biol Soc* 2007: 4312-4315.
10. Garaci FG, Bolacchi F, Cerulli A, Melis M, Spanò A, et al. (2009) Optic nerve and optic radiation neurodegeneration in patients with glaucoma: in vivo analysis with 3-T diffusion-tensor MR imaging. *Radiology* 252: 496-501.

11. Engelhorn T, Michelson G, Waerntges S, Struffert T, Haider S, et al. (2011) Diffusion tensor imaging detects rarefaction of optic radiation in glaucoma patients. *Acad Radiol* 18: 764-769.
12. Hood DC, Anderson SC, Wall M, Raza AS, Kardon RH (2009) A test of a linear model of glaucomatous structure-function loss reveals sources of variability in retinal nerve fiber and visual field measurements. *Invest Ophthalmol Vis Sci* 50: 4254-4266.
13. Smith SM, Jenkinson M, Woolrich MW, Beckmann CF, Behrens TE, et al. (2004) Advances in functional and structural MR image analysis and implementation as FSL. *Neuroimage* 23 Suppl 1: S208-219.
14. Woolrich MW, Jbabdi S, Patenaude B, Chappell M, Makni S, et al. (2009) Bayesian analysis of neuroimaging data in FSL. *Neuroimage* 45: S173-186.
15. Eickhoff SB, Stephan KE, Mohlberg H, Grefkes C, Fink GR, et al. (2005) A new SPM toolbox for combining probabilistic cytoarchitectonic maps and functional imaging data. *Neuroimage* 25: 1325-1335.
16. Bürgel U, Amunts K, Hoemke L, Mohlberg H, Gilsbach JM, et al. (2006) White matter fiber tracts of the human brain: three-dimensional mapping at microscopic resolution, topography and intersubject variability. *Neuroimage* 29: 1092-1105.
17. Vanni S, Henriksson L, James AC (2005) Multifocal fMRI mapping of visual cortical areas. *Neuroimage* 27: 95-105.
18. Yücel YH, Zhang Q, Weinreb RN, Kaufman PL, Gupta N (2003) Effects of retinal ganglion cell loss on magno-, parvo-, koniocellular pathways in the lateral geniculate nucleus and visual cortex in glaucoma. *Prog Retin Eye Res* 22: 465-481.
19. Stark DD, Bradley WG (1996) Magnetic Resonance Imaging. In: Scott W (Ed) *Orbit*. Mosby, Missouri, pp: 988-1028.
20. Zhang YQ, Li J, Xu L, Zhang L, Wang ZC, et al. (2012) Anterior visual pathway assessment by magnetic resonance imaging in normal-pressure glaucoma. *Acta Ophthalmol* 90: e295-302.
21. Kashiwagi K, Okubo T, Tsukahara S (2004) Association of magnetic resonance imaging of anterior optic pathway with glaucomatous visual field damage and optic disc cupping. *J Glaucoma* 13: 189-195.
22. Lagrèze WA, Gaggl M, Weigel M, Schulte-Mönting J, Bühler A, et al. (2009) Retrobulbar optic nerve diameter measured by high-speed magnetic resonance imaging as a biomarker for axonal loss in glaucomatous optic atrophy. *Invest Ophthalmol Vis Sci* 50: 4223-4228.
23. Nucci C, Mancino R, Martucci A, Bolacchi F, Manenti G, et al. (2012) 3-T Diffusion tensor imaging of the optic nerve in subjects with glaucoma: correlation with GDx-VCC, HRT-III and Stratus optical coherence tomography findings. *Br J Ophthalmol* 96: 976-980.
24. Hood DC, Anderson SC, Wall M, Kardon RH (2007) Structure versus function in glaucoma: an application of a linear model. *Invest Ophthalmol Vis Sci* 48: 3662-3668.
25. Knight OJ, Chang RT, Feuer WJ, Budenz DL (2009) Comparison of retinal nerve fiber layer measurements using time domain and spectral domain optical coherent tomography. *Ophthalmology* 116: 1271-1277.
26. Bolacchi F, Garaci FG, Martucci A, Meschini A, Fornari M, et al. (2012) Differences between Proximal versus Distal Intraorbital Optic nerve Diffusion Tensor Magnetic Resonance Imaging Properties in Glaucoma Patients. *Invest Ophthalmol Vis Sci* 53: 4191-4196.
27. Landers J, Tang KC, Hing S (2004) A visual field abnormality: ocular or cerebral cause? *Clin Experiment Ophthalmol* 32: 219-222.
28. Suzuki J, Tomidokoro A, Araie M, Tomita G, Yamagami J, et al. (2004) Visual field damage in normal-tension glaucoma patients with or without ischemic changes in cerebral magnetic resonance imaging. *Jpn J Ophthalmol* 48: 340-344.
29. Qing G, Zhang S, Wang B, Wang N (2010) Functional MRI signal changes in primary visual cortex corresponding to the central normal visual field of patients with primary open-angle glaucoma. *Invest Ophthalmol Vis Sci* 51: 4627-4634.
30. Lu K, Perthen JE, Duncan RO, Zangwill LM, Liu TT (2008) Noninvasive measurement of the cerebral blood flow response in human lateral geniculate nucleus with arterial spin labeling fMRI. *Hum Brain Mapp* 29: 1207-1214.
31. Fitzgerald MJT, Folan-Curran J (2002) Central Visual Pathways. In: Fitzgerald MJT, Folan-Curran J (Eds) *Clinical Neuroanatomy and Related Neuroscience*. (4th edn), W.B.Saunders, Spain, pp: 231-240.
32. Mukherjee P, Miller JH, Shimony JS, Philip JV, Nehra D, et al. (2002) Diffusion-tensor MR imaging of gray and white matter development during normal human brain maturation. *AJNR Am J Neuroradiol* 23: 1445-1456.
33. Granziera C, DaSilva AF, Snyder J, Tuch DS, Hadjikhani N (2006) Anatomical alterations of the visual motion processing network in migraine with and without aura. *PLoS Med* 3: e402.
34. Chidlow G, Wood JP, Casson RJ (2007) Pharmacological neuroprotection for glaucoma. *Drugs* 67: 725-759.
35. Durand CP (2013) Does raising type 1 error rate improve power to detect interactions in linear regression models? A simulation study. *PLoS One* 8: e71079.